

## Path Integral Monte Carlo Calculation of the Deuterium Hugoniot

B. Militzer and D. M. Ceperley

Department of Physics, National Center for Supercomputing Applications, University of Illinois at Urbana-Champaign,  
Urbana, Illinois 61801

(Received 24 January 2000)

Restricted path integral Monte Carlo simulations have been used to calculate the equilibrium properties of deuterium for two densities: 0.674 and 0.838 g cm<sup>-3</sup> ( $r_s = 2.00$  and 1.86) in the temperature range of  $10^5 \leq T \leq 10^6$  K. We carefully assess size effects and dependence on the time step of the path integral. Further, we compare the results obtained with a free particle nodal restriction with those from a self-consistent variational principle, which includes interactions and bound states. By using the calculated internal energies and pressures, we determine the shock Hugoniot and compare with recent laser shock wave experiments as well as other theories.

PACS numbers: 62.50.+p, 02.70.Lq, 05.30.-d

*I. Introduction.*—Recent laser shock wave experiments on precompressed liquid deuterium [1,2] have produced an unexpected equation of state for pressures up to 3.4 Mbar. It was found that deuterium has a significantly higher compressibility than predicted by the semiempirical equation of state based on plasma many-body theory and lower pressure shock data (see SESAME model [3]). These experiments have triggered theoretical efforts to understand the state of compressed hydrogen in this range of density and temperature, made difficult because the experiments are in a regime where strong correlations and a significant degree of electron degeneracy are present. At this high density, it is problematic even to define the basic units such as molecules, atoms, free deuterons, and electrons. Conductivity measurements [2] as well as theoretical estimates [4,5] suggest that, in the experiment, a state of significant but not complete metallization was reached.

A variety of simulation techniques and analytical models have been advanced to describe hydrogen in this particular regime. There are *ab initio* methods such as restricted path integral Monte Carlo (PIMC) simulations [5–7] and density functional theory molecular dynamics (DFTMD) [8,9]. Further, there are models [4,10,11] that minimize an approximate free energy function constructed from known theoretical limits with respect to the chemical composition.

We present results from new, more accurate, PIMC simulations to calculate properties on the shock Hugoniot. We performed a finite size and time step study using a parallelized PIMC code that allowed simulation of twice the number of particles with  $N_P = 64$  pairs of electrons and deuterons and decreased the time step by a factor of 8 ( $\tau^{-1} = 10^6$  K to  $\tau^{-1} = 8 \times 10^6$  K) compared to earlier simulations [7]. More importantly, we studied the effect of the nodal restriction on the Hugoniot by introducing a variational density matrix (VDM) [12] and compare results from free particle (FP) nodes used in [7].

*II. Restricted path integrals.*—The density matrix (DM) of a quantum system at temperature  $k_B T = 1/\beta$  can be written as an integral over all paths  $\mathbf{R}_t$ ,

$$\rho(\mathbf{R}_0, \mathbf{R}_\beta; \beta) = \frac{1}{N!} \sum_{\mathcal{P}} (\pm 1)^{\mathcal{P}} \oint_{\mathbf{R}_0 \rightarrow \mathcal{P}\mathbf{R}_\beta} d\mathbf{R}_t e^{-S[\mathbf{R}_t]}. \quad (1)$$

$\mathbf{R}_t$  stands for the entire paths of  $N$  particles in three-dimensional space  $\mathbf{R}_t = (\mathbf{r}_{1t}, \dots, \mathbf{r}_{Nt})$  beginning at  $\mathbf{R}_0$  and connecting to  $\mathcal{P}\mathbf{R}_\beta$ .  $\mathcal{P}$  labels the permutation of the particles. The upper sign corresponds to a system of bosons and the lower one corresponds to fermions. For nonrelativistic particles interacting with a potential  $V(\mathbf{R})$ , the action of the path  $S[\mathbf{R}_t]$  is given by

$$S[\mathbf{R}_t] = \int_0^\beta dt \left[ \frac{m}{2} \left| \frac{d\mathbf{R}(t)}{\hbar dt} \right|^2 + V[\mathbf{R}(t)] \right] + \text{const}. \quad (2)$$

One can estimate quantum mechanical expectation values using Monte Carlo simulations [13] with a finite number of imaginary time slices  $M$  corresponding to a *time step*  $\tau = \beta/M$ .

For fermionic systems the integration is complicated due to the cancellation of positive and negative contributions to the integral (*the fermion sign problem*). It can be shown that the efficiency of the straightforward implementation scales like  $e^{-2\beta N f}$ , where  $f$  is the free energy difference per particle of a corresponding fermionic and bosonic system [14]. In [14,15], it has been shown that one can evaluate the path integral by restricting the path to only specific positive contributions. One introduces a reference point  $\mathbf{R}^*$  on the path that specifies the nodes of the DM,  $\rho(\mathbf{R}, \mathbf{R}^*, t) = 0$ . A *node-avoiding* path for  $0 < t \leq \beta$  neither touches nor crosses a node:  $\rho[\mathbf{R}(t), \mathbf{R}^*, t] \neq 0$ . By restricting the integral to node-avoiding paths,

$$\rho_F(\mathbf{R}_\beta, \mathbf{R}^*; \beta) = \int d\mathbf{R}_0 \rho_F(\mathbf{R}_0, \mathbf{R}^*; 0) \times \oint_{\mathbf{R}_0 \rightarrow \mathbf{R}_\beta \in Y(\mathbf{R}^*)} d\mathbf{R}_t e^{-S[\mathbf{R}_t]}, \quad (3)$$

[ $Y(\mathbf{R}^*)$  denotes the restriction], the contributions are positive and therefore PIMC represents, in principle, a solution to the sign problem. The method is exact if the exact fermionic DM is used for the restriction. However, the exact DM is known only in a few cases. In practice, applications have approximated the fermionic DM, by a determinant of single particle DMs,

$$\rho(\mathbf{R}, \mathbf{R}'; \beta) = \begin{vmatrix} \rho_1(\mathbf{r}_1, \mathbf{r}'_1; \beta) & \dots & \rho_1(\mathbf{r}_N, \mathbf{r}'_1; \beta) \\ \vdots & \ddots & \vdots \\ \rho_1(\mathbf{r}_1, \mathbf{r}'_N; \beta) & \dots & \rho_1(\mathbf{r}_N, \mathbf{r}'_N; \beta) \end{vmatrix}. \quad (4)$$

This approach has been extensively applied using the FP nodes [14],

$$\rho_1(\mathbf{r}, \mathbf{r}', \beta) = (4\pi\lambda\beta)^{-3/2} \exp\{-(\mathbf{r} - \mathbf{r}')^2/4\lambda\beta\} \quad (5)$$

with  $\lambda = \hbar^2/2m$ , including applications to dense hydrogen [5–7]. It can be shown that for temperatures larger than the Fermi energy the interacting nodal surface approaches the FP nodal surface. In addition, in the limit of low density, exchange effects are negligible, the nodal constraint has a small effect on the path and therefore its precise shape is not important. The FP nodes also become exact in the limit of high density when kinetic effects dominate over the interaction potential. However, for the densities and temperatures under consideration, interactions could have a significant effect on the fermionic DM.

To gain some quantitative estimate of the possible effect of the nodal restriction on the thermodynamic properties, it is necessary to try an alternative. In addition to FP nodes, we used a restriction taken from a VDM that already includes interactions and atomic and molecular bound states.

The VDM is a variational solution of the Bloch equation. Assume a trial DM with parameters  $q_i$  that depend on imaginary time  $\beta$  and  $\mathbf{R}'$ ,

$$\rho(\mathbf{R}, \mathbf{R}'; \beta) = \rho(\mathbf{R}, q_1, \dots, q_m). \quad (6)$$

By minimizing the integral

$$\int d\mathbf{R} \left( \frac{\partial \rho(\mathbf{R}, \mathbf{R}'; \beta)}{\partial \beta} + \mathcal{H} \rho(\mathbf{R}, \mathbf{R}'; \beta) \right)^2 = 0, \quad (7)$$

one determines equations for the dynamics of the parameters in imaginary time:

$$\frac{1}{2} \frac{\partial H}{\partial \vec{q}} + \vec{\mathcal{N}} \dot{\vec{q}} = 0 \quad \text{where } H \equiv \int \rho \mathcal{H} \rho d\mathbf{R}. \quad (8)$$

The normalization matrix is

$$\mathcal{N}_{ij} = \lim_{q' \rightarrow q} \frac{\partial^2}{\partial q_i \partial q'_j} \left[ \int d\mathbf{R} \rho(\mathbf{R}, \vec{q}; \beta) \rho(\mathbf{R}, \vec{q}'; \beta) \right]. \quad (9)$$

We assume that the DM is a Slater determinant of single particle Gaussian functions

$$\rho_1(\mathbf{r}, \mathbf{r}', \beta) = (\pi w)^{-3/2} \exp\{-(\mathbf{r} - \mathbf{m})^2/w + d\}, \quad (10)$$

where the variational parameters are the mean  $\mathbf{m}$ , squared width  $w$ , and amplitude  $d$ . The differential equation for this ansatz is given in [12]. The initial conditions at  $\beta \rightarrow 0$  are  $w = 2\beta$ ,  $\mathbf{m} = \mathbf{r}'$ , and  $d = 0$  in order to regain the correct FP limit. It follows from Eq. (7) that, at low temperature, the VDM goes to the lowest energy wave function within the variational basis. For an isolated atom or molecule this will be a bound state, in contrast to the delocalized state of the FP DM. A further discussion of the VDM properties is given in [12]. Note that this discussion concerns only the nodal restriction. In performing the PIMC simulation, the complete potential between the interacting charges is taken into account as discussed in detail in [13].

Simulations with VDM nodes lead to lower internal energies than those with FP nodes, as shown in Fig. 1. Since the free energy  $F$  is the integral of the internal energy over temperature, one can conclude that VDM nodes yield to a smaller  $F$  and, hence, are the more appropriate nodal surface.

For the two densities considered here, the state of deuterium goes from a plasma of strongly interacting but unbound deuterons and electrons at high  $T$  to a regime at low  $T$ , which is characterized by a significant electronic degeneracy and bound states. Also, at decreasing  $T$ , one finds an increasing number of electrons involved in long permutation cycles. Additionally for  $T \leq 15\,625$  K, molecular formation is observed. By comparing FP and VDM nodes, one finds that VDM predicts a higher molecular fraction and fewer permutations, suggesting more localized electrons.

*III. Shock Hugoniot.*—The recent experiments measured the shock velocity, propagating through a sample of precompressed liquid deuterium characterized by an initial state,  $(E_0, V_0, p_0)$  with  $T = 19.6$  K and  $\rho_0 = 0.171$  g/cm<sup>3</sup>. Assuming an ideal planar shock front, the variables of the shocked material  $(E, V, p)$  satisfy the Hugoniot relation [16],

$$H = E - E_0 + \frac{1}{2}(V - V_0)(p + p_0) = 0. \quad (11)$$

We set  $E_0$  to its exact value of  $-15.886$  eV per atom [17] and  $p_0 = 0$ . Using the simulation results for  $p$  and

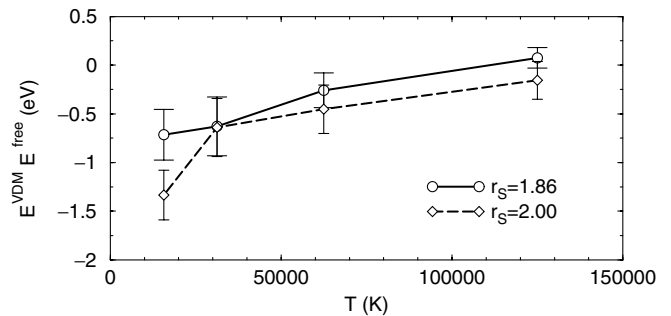


FIG. 1. Difference in the internal energy per atom from PIMC simulations with VDM and FP nodes vs temperature using  $N_p = 32$  and  $\tau^{-1} = 2 \times 10^6$  K.

TABLE I. Pressure and internal energy per atom and the resulting Hugoniot from PIMC simulations with 32 pairs of particles. For  $T \geq 250\,000$  K, we list results with FP nodes,  $\tau_F^{-1} = 8 \times 10^6$  K, and  $\tau_B^{-1} = 2 \times 10^6$  K, otherwise with VDM nodes and  $\tau^{-1} = 2 \times 10^6$  K.

$T(K)$	$p$ (Mbar) $r_s = 2$	$E$ (eV) $r_s = 2$	$p$ (Mbar) $r_s = 1.86$	$E$ (eV) $r_s = 1.86$	$\rho^{\text{Hug}}$ ( $\text{g cm}^{-3}$ )	$\rho^{\text{Hug}}$ (Mbar)
1 000 000	53.79 (5)	245.7 (3)	66.85 (8)	245.3 (4)	0.7019 (01)	56.08 (5)
500 000	25.98 (4)	113.2 (2)	32.13 (5)	111.9 (2)	0.7130 (01)	27.48 (4)
250 000	12.12 (3)	45.7 (2)	14.91 (3)	44.3 (2)	0.7242 (01)	12.99 (2)
125 000	5.29 (4)	11.5 (2)	6.66 (2)	11.0 (1)	0.7300 (03)	5.76 (2)
62 500	2.28 (4)	-3.8 (2)	2.99 (4)	-3.8 (2)	0.7334 (11)	2.54 (3)
31 250	1.11 (6)	-9.9 (3)	1.58 (7)	-9.7 (3)	0.7328 (26)	1.28 (5)
15 625	0.54 (5)	-12.9 (3)	1.01 (5)	-12.0 (2)	0.7210 (35)	0.68 (4)
10 000	0.47 (5)	-13.6 (3)	0.80 (8)	-13.2 (4)	0.6920 (60)	0.51 (5)

$E$ , we calculate  $H(T, \rho)$  and then interpolate  $H$  linearly at constant  $T$  between the two densities corresponding to  $r_s = 1.86$  and 2 to obtain a point on the Hugoniot in the  $(p, \rho)$  plane. (Results at  $r_s = 1.93$  confirm that the function is linear within the statistical errors). The PIMC data for  $p$ ,  $E$ , and the Hugoniot are given in Table I.

In Fig. 2, we compare the effects of different approximations made in the PIMC simulations such as time step  $\tau$ , number of pairs  $N_P$ , and the type of nodal restriction. For pressures above 3 Mbar, all of these approximations have a very small effect. The reason is that PIMC simulations become increasingly accurate as temperature increases. The first noticeable difference occurs at  $p \approx 2.7$  Mbar, which

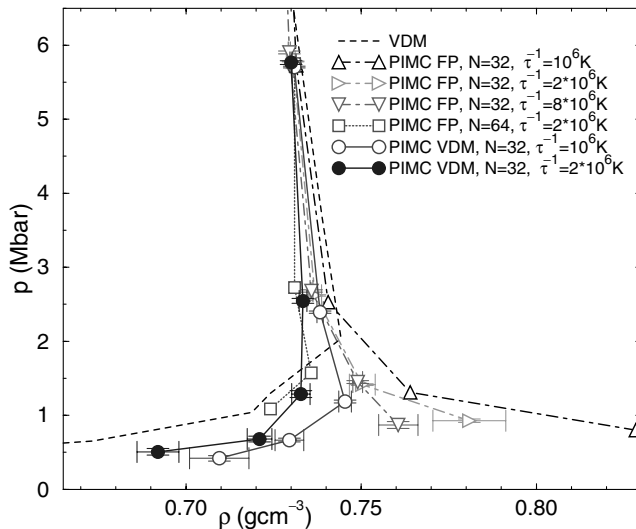


FIG. 2. Comparison of the Hugoniot calculated with PIMC simulations of different accuracy: FP nodes with  $N_P = 32$  ( $\Delta$  for  $\tau^{-1} = 10^6$  K reported in [5],  $\nabla$  for  $\tau^{-1} = 2 \times 10^6$  K,  $\nabla$  for  $\tau_F^{-1} = 8 \times 10^6$  K and  $\tau_B^{-1} = 2 \times 10^6$  K) and  $N_P = 64$  ( $\square$  for  $\tau^{-1} = 2 \times 10^6$  K) as well as with VDM nodes and  $N_P = 32$  ( $\circ$  for  $\tau^{-1} = 10^6$  K and  $\bullet$  for  $\tau^{-1} = 2 \times 10^6$  K). Beginning at high pressures, the points on each Hugoniot correspond to the following temperatures 125 000, 62 500, 31 250, 15 625, and for the PIMC VDM curves also to 10 000 K. The dashed line corresponds to a calculation using the VDM alone.

corresponds to  $T = 62\,500$  K. At lower pressures, the differences become more and more pronounced. We have performed simulations with FP nodes and  $N_P = 32$  for three different values of  $\tau$ . A smaller time step shifts the Hugoniot curves to lower densities. These differences come mainly from enforcing the nodal surfaces more accurately, which seems to be more relevant than the improvements in the accuracy of the action  $S$ . That is, the time step is constrained more by the Fermi statistics than by the potential energy. We improved the efficiency of the algorithm by using a smaller time step  $\tau_F$  for evaluating the Fermi action than the time step  $\tau_B$  used for the potential action. Unless specified otherwise, we used  $\tau_F = \tau_B = \tau$ .

As a next step, we replaced the FP nodes by VDM nodes. Those results show that the form of the nodes has a significant effect on  $p$  below 2 Mbar. Using a smaller  $\tau$  also shifts the curve to slightly lower densities. In the region where atoms and molecules are forming, it is plausible that VDM nodes are more accurate than FP nodes because they can describe those states [12]. We also show a Hugoniot derived on the basis of the VDM alone. These results are quite reasonable considering the approximations (Hartree-Fock) made in that calculation. Therefore, we consider the PIMC simulation with the smallest time step using VDM nodes ( $\bullet$ ) to be our most reliable Hugoniot. Going to bigger system sizes  $N_P = 64$  and using FP nodes also show a shift towards lower densities. The FP size dependence becomes larger at lower temperatures because the pressure is increasingly sensitive to structural changes involving the formation and dissociation of molecules.

Figure 3 compares the Hugoniot from Laser shock wave experiments [1,2] with PIMC simulation (VDM nodes,  $\tau^{-1} = 2 \times 10^6$  K) and several theoretical approaches: SESAME model by Kerley [3] (thin solid line), linear mixing model by Ross (dashed line) [4], DFTMD by Lenosky *et al.* [8] (dashed-dotted line), Padé approximation in the chemical picture (PACH) by Ebeling *et al.* [11] (dotted line), and the work by Saumon *et al.* [10] (thin dashed-dotted line).

The differences of the various PIMC curves in Fig. 2 are small compared to the deviation from the experimental

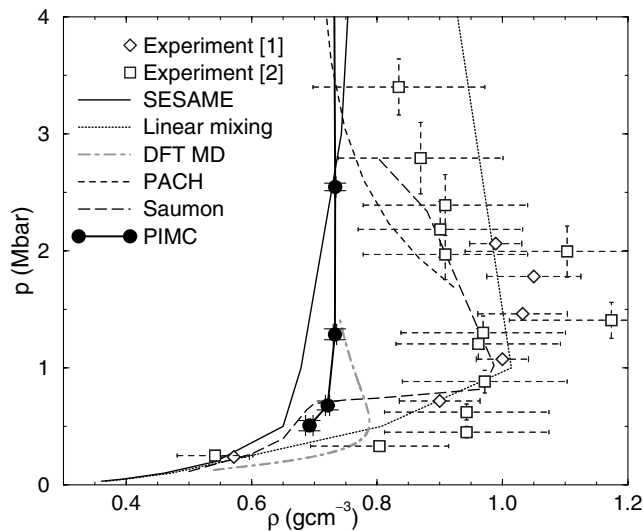


FIG. 3. Comparison of experimental and several theoretical Hugoniot. The PIMC curve was calculated with VDM nodes,  $\tau^{-1} = 2 \times 10^6$  K, and 32 particle pairs.

results [1,2]. There, an increased compressibility with a maximum value of  $6 \pm 1$  was found, while PIMC predicts  $4.3 \pm 0.1$ , only slightly higher than that given by the SESAME model. Our Hugoniot lies within experimental error bars only for  $p > 2.5$  Mbar. In this regime, the deviations in the PIMC and PACH Hugoniot are relatively small, less than  $0.05 \text{ g cm}^{-3}$  in density. In the high pressure limit, the Hugoniot goes to the FP limit of fourfold compression. This trend is also present in the experimental findings. For pressures below 1 Mbar, the PIMC Hugoniot goes back to lower densities and shows the expected tendency towards the experimental values from earlier gas gun work [18,19] and lowest data points from [1,2]. For these low pressures, differences between PIMC and DFTMD are also relatively small.

*IV. Conclusions.*—We reported results from PIMC simulations and performed a finite size and time step study. Special emphasis was put on improving the fermion nodes where we presented the first PIMC results with variational instead of FP nodes. We find a slightly increased compressibility of  $4.3 \pm 0.1$  compared to the SESAME model, but we cannot reproduce the experimen-

tal findings of values of about  $6 \pm 1$ . Further theoretical and experimental work will be needed to resolve this discrepancy.

The authors would like to thank W. Magro, for collaboration concerning the parallel PIMC simulations, and E. L. Pollock, for contributions to the VDM method. This research was funded by the U.S. Department of Energy through the University of California under Subcontract No. B341494. We used the computational facilities at the National Center for Supercomputing Applications and Lawrence Livermore National Laboratories.

- 
- [1] L. B. Da Silva *et al.*, Phys. Rev. Lett. **78**, 483 (1997).
  - [2] G. W. Collins *et al.*, Science **281**, 1178 (1998).
  - [3] G. I. Kerley, *Molecular Based Study of Fluids* (ACS, Washington, D.C., 1983), p. 107.
  - [4] M. Ross, Phys. Rev. B **58**, 669 (1998).
  - [5] B. Militzer, W. Magro, and D. Ceperley, Contrib. Plasma Phys. **39**, 151 (1999).
  - [6] C. Pierleoni, D. M. Ceperley, B. Bernu, and W. R. Magro, Phys. Rev. Lett. **73**, 2145 (1994).
  - [7] W. R. Magro, D. M. Ceperley, C. Pierleoni, and B. Bernu, Phys. Rev. Lett. **76**, 1240 (1996).
  - [8] T. J. Lenosky, S. R. Bickham, J. D. Kress, and L. A. Collins, Phys. Rev. B **61**, 1 (2000).
  - [9] G. Galli, R. Q. Hood, A. U. Hazi, and F. Gygi, Phys. Rev. B **61**, 909 (2000).
  - [10] D. Saumon, G. Chabrier, and H. M. Van Horn, Astrophys. J. **99**, 713 (1995).
  - [11] W. Ebeling and W. Richert, Phys. Lett. **108A**, 85 (1985).
  - [12] B. Militzer and E. L. Pollock, Phys. Rev. E **61**, 3470 (2000).
  - [13] D. M. Ceperley, Rev. Mod. Phys. **67**, 279 (1995).
  - [14] D. M. Ceperley, *Monte Carlo and Molecular Dynamics of Condensed Matter Systems* (Editrice Compositori, Bologna, Italy, 1996).
  - [15] D. M. Ceperley, J. Stat. Phys. **63**, 1237 (1991).
  - [16] Y. B. Zeldovich and Y. P. Raizer, *Physics of Shock Waves and High-Temperature Hydrodynamic Phenomena* (Academic Press, New York, 1966).
  - [17] W. Kolos and L. Wolniewicz, J. Chem. Phys. **41**, 3674 (1964).
  - [18] W. J. Nellis *et al.*, J. Chem. Phys. **79**, 1480 (1983).
  - [19] N. C. Holmes, M. Ross, and W. J. Nellis, Phys. Rev. B **52**, 15 835 (1995).